Analytic dynamics of the one-dimensional tight-binding model. III. Numerical studies

1989 J. Phys.: Condens. Matter 1 6793

(http://iopscience.iop.org/0953-8984/1/38/004)

J. Phys.: Condens. Matter 1 (1989) 6793–6806. Printed in the UK

Analytic dynamics of the one-dimensional tight-binding model: III. Numerical studies

M A Brackstone† and S W Lovesey‡

† Department of Physics, University of Southampton, Highfield, Southampton SO9 5NH, UK

‡ Rutherford Appleton Laboratory, Chilton, Didcot, Oxfordshire OX11 0QX, UK

Received 3 January 1989

Abstract. Properties of electron dynamics in a magnetic field and spin fluctuations in a modulated magnet are studied by implementing formulae for response functions derived in two previous papers. Results for the electron band structure and density of states are reported for a wide range of rational magnetic fields and (tight-binding) band-structure parameters. The special features of spin fluctuations in longitudinally modulated magnets are reported in terms of the transverse dynamic susceptibility observed in inelastic neutron scattering experiments.

1. Introduction

The topic of incommensurate systems, characterised by the presence of two relevant length scales which in general do not form a rational fraction, has many features that intrigue both theorists and experimentalists, Realisations include band electrons in a magnetic field, spin fluctuations in longitudinally modulated magnets and adsorbed monolayers. For reviews see Simon (1982), Sokoloff (1985) and Currat and Janssen (1988).

In two previous papers (Lovesey 1988a, b) we have addressed the task of deriving the analytic dynamics of the standard models for two physically very different systems. One model, which describes electrons in a magnetic field H, is based on Harper's equation, equivalent to the discrete (lattice) version of Mathieu's equation, for the eigen-function ψ_n, namely

$$\psi_{n-1} + \psi_{n+1} + 2\gamma \cos(nQ + \Delta)\psi_n = \omega\psi_n. \tag{1.1}$$

Here, the integer n is a site label and Q is the modulation wavevector, proportion to H. The wave equation (1.1) is based on a tight-binding model and incorporation of the magnetic field by the Peierls substitution (minimal coupling).

A numerical investigation of the energy spectrum has been presented by Hofstadter (1976). The previous analytic work (Lovesey 1988a, b) provides a basis for the interpretation of this numerical work, together with formulae for response functions, including the density of states and site-dependent propagator. The analytic work exploits the simplifications that arise for periodic modulations, $Q = 2\pi M/N$, with M and N integers. The latter provides the appropriate theory for understanding numerical simulation

0953-8984/89/386793 + 14 $02.50

work, and successive approximations to truly incommensurate states. If we should choose to look at the electron system experimentally we find that only very small Q values are readily accessible in laboratory magnetic fields with samples currently available (typically 1×10^6 T is required to satisfy $M/N = 1/2$).

Relatively large magnetic fields are experienced by atoms in ordered magnetic materials. An appropriate incommensurate system is a longitudinally modulated magnetic configuration, realised in some rare-earth metals at elevated temperatures. For such systems, Q is typically a significant fraction of π; to a first approximation, neodymium is described by a modulation $Q = \pi/4$.

The standard electron model and our analysis of its dynamic properties are surveyed in § 2. Results for the band structure and density of states are gathered in § 3 for a wide range of parameters. The analogous material for the spin model is presented in §§ 4 and 5. The conclusions are given in § 6.

2. Formalism of the electron model

In paper II (Lovesey 1988b) we looked at the 3D tight-binding model in the presence of a magnetic field, incorporated by minimal (Peierls) coupling. Motion in two orthogonal directions is plane-wave-like, with the dynamics in a third direction, perpendicular to the applied field, described by the one-dimensional Hamiltonian

$$\mathcal{H} = \sum_n |n\rangle\langle n+1| + |n+1\rangle\langle n| + e_n|n\rangle\langle n| \tag{2.1}$$

$$e_n = 2\gamma\cos(nQ + \Delta) \qquad e_{n+N} = e_n,$$

where the eigen-function labelled by α is $\psi_n(\alpha) = \langle n|\alpha\rangle$. The difference equation (1.1) for the orthonormal eigen-functions is readily obtained, by forming $\mathcal{H}|\alpha\rangle$ for example.

The density of states, $Z(\omega)$, for a 1D system in inversely proportional to the group velocity, i.e. to the frequency derivative of the 'Bloch' wavefunction $K(\omega)$. If we have the particular solutions to (1.1), p_m and q_m, ($m-1$-, $m-2$-order polynomials in ω with coefficients being combinations of the $\{e_m\}$, subject to the conditions $p_0 = q_1 = 0$ and $p_1 = q_0 = 1$), then by using Floquet's theorem we obtain the relation

$$2\cos(NK(\omega)) = p_{N+1} + q_N = \theta_N. \tag{2.2}$$

The second equality defines a polynomial θ_N of order N. We find

$$Z(\omega) = \begin{cases} (1/2\pi N)|\theta_N'(\omega)|/D_N^{1/2}(\omega) & D_N \geqslant 0 \\ 0 & D_N < 0 \end{cases} \tag{2.3}$$

where the prime denotes differentiation of θ_N with respect to ω. The quantity D_N, termed the discriminant, is defined to be

$$D_N = 1 - (\theta_N/2)^2. \tag{2.4}$$

For a band we have $\mathrm{Im}\, K = 0$, and Bloch-type eigen-functions, whereas for $|\theta_N| > 2$, $\mathrm{Im}\, K \sim \ln[(\theta_N/2) + \sqrt{-D_N}]$, giving localised states.

Another useful response function is the site representation of the one-particle Green function, formed from the resolvent operator,

$$G(m, n:z) = -\langle m|1/(\mathcal{H} - z)|n\rangle. \tag{2.5}$$

The density of states, for example, is the sum of the imaginary parts of the site-diagonal Green functions. It is straightforward to show from (2.1) that (2.5) satisfies the equation of motion

$$zG(m, n) = \delta_{m,n} + G(m+1, n) + G(m-1, n) + e_m G(m, n) \tag{2.6}$$

which is equivalent to (1.1) apart from the inhomogeneous term, $\delta_{m,n}$, due to the orthonormality of the eigen-functions. The Green function may be expressed in terms of continued fractions, i.e. functions of the form

$$1/e_m - z - 1/(e_{m+1} - z - \ldots)] \tag{2.7}$$

with Re $z = \omega$ and Im $Z \geqslant 0$.

In papers I and II it is shown that, for a periodic system $e_n = e_{n+N}$, the continued fraction can be written in closed form using the polynomials p_m and q_m introduced earlier. Hence, the density of states and Green function are expressed in terms of polynomials which can readily be generated recursively.

3. Results for the electron model

The essential elements of our investigation, the band edges, are the zeros of the discriminant, D_N, of (2.3). We may ask how the band distribution changes with N, what is the scale on which these changes occur, and how new bands appear. The behaviour of our eigen-functions may also be studied with regard to localisation by varying the parameter γ in our polynomials and observing the change of not only the bands, but also the Lyapunov exponent. Lastly, the long-proposed fractal nature of the spectrum can be looked at in a reassuringly simple, and analytically proven, way by forming the integrated density of states from (2.2).

We first reformulate (2.3) to avoid the obvious disadvantage in a numerical scheme of having to evaluate a derivative. This is accomplished by casting the Green function in terms of the partial numerators and denominators (A_m and B_m respectively) of continued fractions like (2.7), of which they are composed. The quantities A_m and B_m are simply related to p_m and q_m, of course, but they are slightly simpler to implement. The density of states to be calculated is

$$Z_N(\omega) \sim \sum_m \mathrm{Im}(G(m, m; \omega)) \tag{3.1}$$

and we obtain the numerically useful alternative form

$$Z_N(\omega) = \frac{1}{\pi N} \frac{\mathrm{sgn}(B_{N-1})}{\sqrt{D_N}} \sum_{m=1}^{N} \frac{1}{\Omega_m^2}$$
$$\times \left\{ A_{m-1} + \left[\frac{B_{m-1}}{B_{N-1}} \left(\frac{B_N - A_{N-1}}{2} \right) \right]^2 + \frac{D_N}{2} \left(\frac{B_{m-1}}{B_{N-1}} \right)^2 \right\}$$
$$\Omega_m = e_0 e_1 e_2 \ldots e_{m-1} \qquad D_N \geqslant 0. \tag{3.2}$$

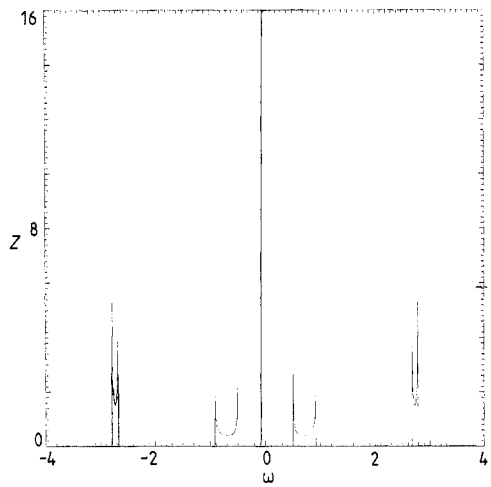

Figure 1. Numerical results for the electronic density of states (DOS) for $M/N = 1/4$, $\gamma = 1$,

It can be shown that (3.2) and (2.3) are identical by observing that the partial numerators, etc, obey the common recursion relation ($R_m \equiv A_m, B_m$):

$$R_m = R_{m-1} - e_{m-1}R_{m-2}$$

which is only a scale factor different from the equation whose solutions are p_m and q_m. Using the Chirstoffel–Darboux relaxation (Akhiezer 1965) between sums of R_m and their derivatives, the relationship between continued fractions and orthogonal polynomials becomes evident.

The basic structure of $Z(\omega)$ is that it is split into N bands, from the $2N$ zeros of D_N. We index the roots λ_i and μ_i (periodic and antiperiodic) according to whether they are the roots of $\theta_N \mp 2 = 0$, respectively. We have shown that the roots form a series of alternating pairs. The maximum width of the spectrum is independent of N. Given that the number of roots is $2N$, the band structure becomes more fragmented with increasing N.

For the moment it is useful to consider the extreme case, $\gamma = 0$, where $N - 1$ of the roots are doubly degenerate, giving a 'connected' spectrum. For example, $M/N = 1/4$, $\gamma = 0$, $D_4 = (\omega^4 - 4\omega^2)(\omega^4 - 4\omega^2 + 4)$ giving coinciding pairs of roots at $\pm\sqrt{2}$ and 0. The exact form of the degeneracy can be obtained from (7.9) of Lovesey (1988b), where we have $\theta_N = 2\cos(N\beta)$ and $\beta = \cos^{-1}(\omega/2)$.

Let us consider a particular non-trivial situation. Choosing the phase, Δ, to be that used in Hofstadter's work ($= -\pi/2N$), we have a symmetric series of roots, where, for N odd, $\lambda_i = \mu_i$, and N even $\mu_i = -\mu_{N+1-i}$. For example, $M/N = 1/4$, $\gamma = 1$:

$$Z_4(\omega) = (1/\pi)\,|\omega(\omega^2 - 4)|/\sqrt{(\omega^4 - 8\omega^2 + 6)(\omega^4 - 8\omega^2 + 2)} \qquad D_4 \geqslant 0 \tag{3.3}$$

as shown in figure 1.

The need for numerical work can be seen when we examine a higher period: here we could recursively generate θ_N, but only after lengthy calculation. The questions addressed below are: (i) the spectral dependence on γ, and (ii) the general form of the band arrangement for a series of different periodicities, M/N (Hofstadter's butterfly).

Choosing for our illustrative example, $M/N = 1/7$, we have the stated root degeneracy at $\gamma = 0$. For other γ values (figure 2) we have the requisite number of independent roots, though some may not be detected, having bandwidths below the resolution of the calculation ($\Delta E = 10^{-2}$). This may be shown by checking the result of some rules

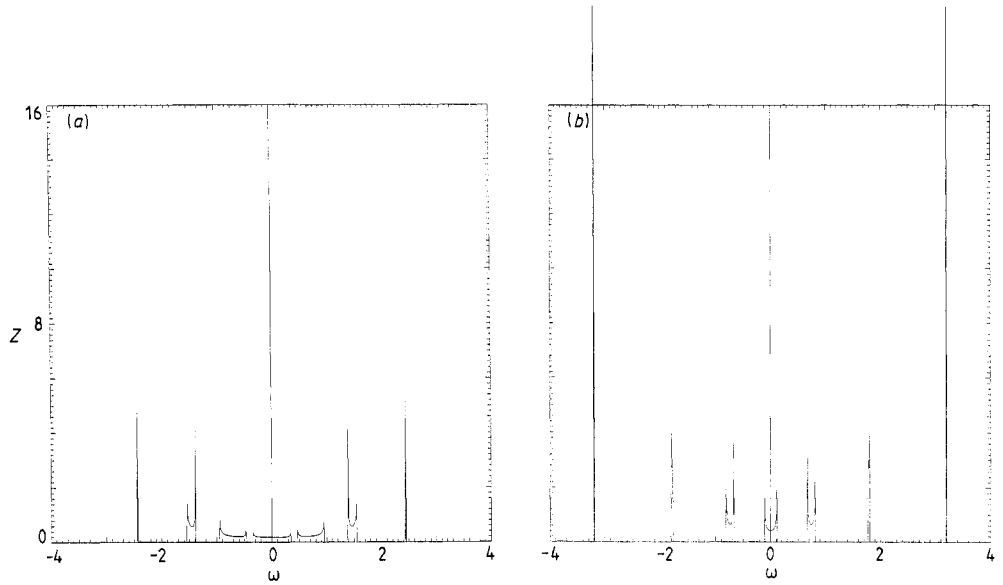

Figure 2. Numerical DOS for $M/N = 1/7$ and (*a*) $\gamma = 0.5$, (*b*) $\gamma = 1.0$.

calculated from the Green function,

$$\int_{-\infty}^{+\infty} -\frac{\mathrm{d}\omega}{\pi}\,\omega^n G(m, n), \tag{3.4}$$

which gives, for example for $n = 2$, the value $2 + e_m^2$. Since for $n = 0$ (3.4) gives unity, we can interpret $n = 2$ as the 'mean square' of the spectrum.

We have cross-checked our results with those of Turchi *et al* (1982). They use a perturbation analysis valid for small γ on a tight-binding Hamiltonian with general hopping/on-site coefficients, with the restriction of giving a two-gap spectrum. Applying this to our Hamiltonian for a periodicity of $N = 3$ with $\gamma \ll 1$, the gaps should be located at approximately $\omega = \pm 1$ and have a width $\sim\gamma$ (figure 3). Also they present exact solutions for a single-gap spectrum. In our corresponding case, $N = 2$, their results predict maximal band edges at $2 \pm 2(1 + \gamma^2/2)^{1/2}$ and a band width of $2\sqrt{2}\gamma$, thus giving a spectrum of vanishing measure as $\gamma \to \infty$ (figure 4).

Another guide is provided by Harper (1955), where a WKB (large-N)-type method is employed on the difference equation for $\gamma = 1$. Harper predicts that the band gaps are roughly the same for the outlying bands which have a narrow width, while, for low energy, the spacing increases and the bands rapidly broaden. For a comparatively low N, the band-gap observation is obviously hard to verify.

To look at the full effect of periodicity on the energy spectra, we produce 'Hofstadter's butterfly' for a range of rational fractions M/N. In the original work this was produced by diagonalising a system of transfer matrices. Our procedure is to find the zeros of the discriminant, D_N, using a Sturmian process with resolution $\Delta E = 5 \times 10^{-4}$ (higher than previously, to ensure that the full forms of the spectra are plotted and appreciated). Our results (figure 5)are similar to those presented by Hofstadter in that the spectra, visually, seem to form a self-similar, Cantor-type process. Some measure of the highly fragmented, close-spaced structure can be gauged from our quadratic and quartic sum rules. The greater the discrepancy, the more bands (band gaps) with a

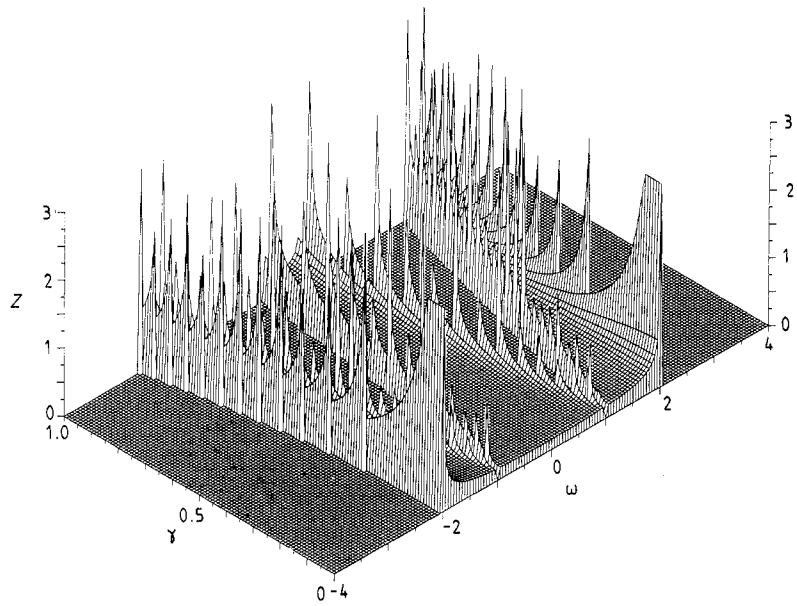

Figure 3. Isometric plot of DOS for $M/N = 1/3$.

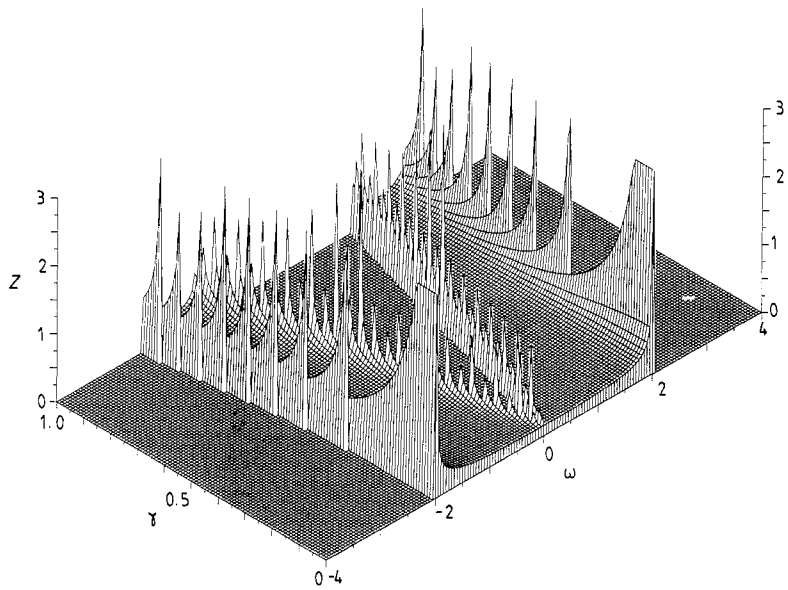

Figure 4. Isometric DOS for $M/N = 1/2$.

measure $|\mu_i - \lambda_i|$ ($|\mu_i - \mu_{i+1}|$) or $|\lambda_i - \lambda_{i+1}|$) less than our resolution we have missed. As is obvious by now, this will be the case for large N (in accordance with Harper's results). We have also obtained plots for other values of γ (figure 6) which confirm our observations at lower N; a broadening of the bands and a 'bunching' of the spectrum for $\gamma < 1$, and the opposite for $\gamma > 1$. For extreme values this produces a noticeable effect. By $\gamma = 0.5$ a visual band merging has started to occur (i.e. small band gaps, if plotable

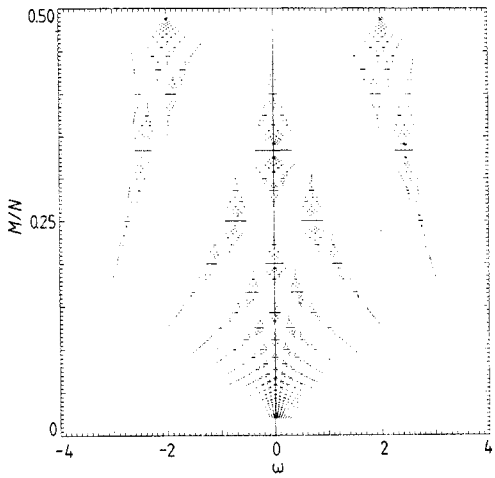

Figure 5. The Hofstadter butterfly: M/N against ω for $\gamma = 1.0$.

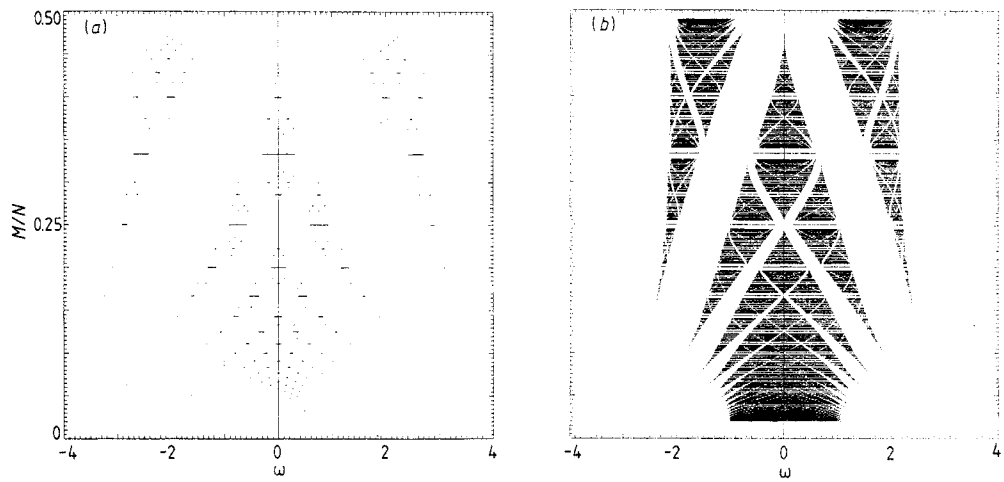

Figure 6. 'Hofstadter moths': M/N against ω for $(a) = 0.5$ and (b) $\gamma = 1.1$.

at all!), alternatively by $\gamma = 1.1$ we have 'thinning' producing a very sparse picture due to 'vanishing' bandwidths. From Turchi's work we are also given a bounding equality for the bandwidth, $W_N = \max(\lambda_{2N}, \mu_{2N}) - \min(\lambda_1, \mu_1)$, and the total measure of the spectrum

$$\eta_n = \sum_i |\mu_i - \lambda_i|$$

namely

$$\begin{aligned} &W_N - \eta_N \geqslant 2|e_n| \qquad \eta_N \leqslant 4 \leqslant 2W_N - \eta_N \\ &\max|e_n| = 2\gamma\cos(\pi/2N) \end{aligned} \tag{3.5}$$

which are satisfied by our $N = 2$ expressions. We also verify these numerically for low N in table 1.

Table 1. Equalities (3..5) for $\gamma = 1$ and various low N for $M = 1$.

N	W_N	η_N	$2\max\|e_n\| \leqslant W_N - \eta_N$		$2W_N - \eta_N$
2	4.90	2.07	2.83	2.83	7.73
3	5.20	1.36	3.46	3.84	9.04
4	5.56	1.03	3.70	4.53	10.09
5	5.90	0.82	3.80	5.08	10.98
7	6.40	0.58	3.90	5.82	12.22

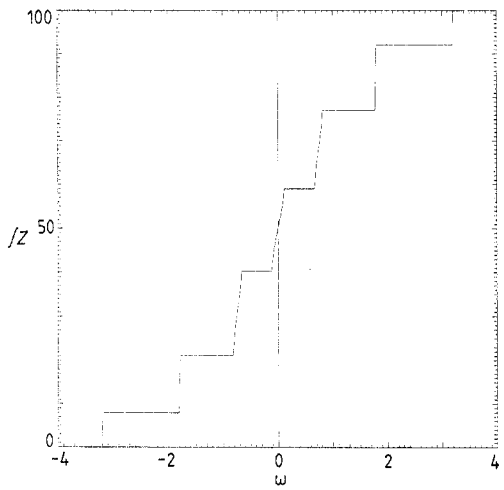

Figure 7. Analytically integrated DOS for $M/N = 1/7$, $\gamma = 1.0$.

Another, traditional, way of displaying multiband behaviour is the integrated density of states (IDS). We may perform this evaluation in two ways.

(i) Numerical integration. Here we face the problem of area approximation to a function that is already inaccurate, in that we do not pick up all the intensity per band, due to our finite bin widths; in fact, with increasing N and γ, we stand a growing chance of missing areas of a high spectral weight altogether!

(ii) Integrating (2.3) analytically gives us an exact expression for the contribution to the IDS at any point within a band; it is constant in the gaps, between our 'steps'. In our evaluation we take care to distinguish which factor in D_N is identified with a root of our polynomial,

$$2 + \theta_N(\mu_i) = 2 - \theta_N(\lambda_i) = 0.$$

One observation we make is that the addition from each band is $1/N$, independent of the size and form of the polynomial $|\theta_N'|\sqrt{D_N}$, in the interval

$$\left|\int_{\mu_i}^{\lambda_i} Z(\omega)\,\mathrm{d}\omega\right| = \frac{1}{\pi N}\left|\cos^{-1}(\theta_N/2)\right|_{\mu_i}^{\lambda_i}$$

$$= \frac{1}{\pi N}\left|\cos^{-1}(-1) - \cos^{-1}(1)\right| = \frac{1}{N} \tag{3.6}$$

which, as there are N bands, gives us a normalised density of states (figure 7).

Exacting questions can now be asked with regard to the Cantor form and measure in the incommensurate limits. These points will be taken up in § 6.

4. Spin fluctuations

The second model that we examine is similar to the much studied ANNNI model. Our model is a Heisenberg, rather than an Ising, magnet, with competing neighbour and next-nearest-neighbour interactions along one axis. The spin Hamiltonian is

$$\mathcal{H} = -\tfrac{1}{2}\sum_{k} [J(\boldsymbol{k})(S_{\boldsymbol{k}}^{+}S_{\boldsymbol{k}}^{-} + S_{\boldsymbol{k}}^{-}S_{\boldsymbol{k}}^{+}) + 2K(\boldsymbol{k})S_{\boldsymbol{k}}^{z}S_{-\boldsymbol{k}}^{z}] \tag{4.1}$$

with

$$J(\boldsymbol{k}) = J_0\,[\cos(\boldsymbol{a}\cdot\boldsymbol{k}) + \cos(\boldsymbol{b}\cdot\boldsymbol{k})] + J_1\cos(\boldsymbol{c}\cdot\boldsymbol{k}) + J_2\cos(2\boldsymbol{c}\cdot\boldsymbol{k}).$$

A molecular-field approximation, where we have $\boldsymbol{k}$ parallel to our 'easy Q' axis, gives an Elliott (1961)-type ground state with

$$\text{for}\qquad \begin{aligned} &\langle S_r^z\rangle = S\cos(\boldsymbol{Q}\cdot\boldsymbol{r}) \\ &J_1/J_2 = -4\cos(Q). \end{aligned} \tag{4.2}$$

Using a linear approximation and S as a temperature-dependent quantity in the equation of motion is equivalent to a Boson prescription for the spin operators:

$$[S_{k+nQ}^{+}, S_{k+mQ}^{-}] = S(\delta_{n,m+1} + \delta_{n,m-1}). \tag{4.3}$$

From this point we can swiftly derive an equivalent expression to (2.6) for the wave-vector-dependent transverse spin Green function, with our diagonal term replaced by the off-diagonal coupling of (4.3):

$$\omega G(m,n) = S(\delta_{m,n+1} + \delta_{m,n-1}) + W_{m-1}G(m-1,n) + W_{m+1}G(m+1,n) \tag{4.4}$$

where W_m are energy coefficients (in units of $S(D + J_1\cos Q + J_2\cos 2Q)$):

$$W_m = 1 + \alpha\cos(k + mQ) + \beta\cos(2(k + mQ)) \tag{4.5}$$

$$\alpha/\beta = J_1/J_2 = -4\cos(Q).$$

Expanding our spin operators in terms of eigen-states of our equations of motion, we find

$$b_\alpha = \sum_n f_\alpha(n)S_n^{+}\,(W_n/S)^{1/2} \tag{4.6}$$

where

$$[b_\alpha, b_\beta^{+}] = \omega\delta_{\alpha,\beta}. \tag{4.7}$$

The static susceptibility is found to be

$$\chi_0(k) = \frac{-2}{\pi}\int\frac{\mathrm{d}\,\omega}{\omega}\,G''(m,m;\omega) = \frac{2S}{W_0} \geqslant 0. \tag{4.8}$$

As χ_0 is necessarily non-negative, we are able to impose physical restrictions on α and β. From (4.8) we note that $\chi_0(k)$ has a maximum for $k = Q$, giving

$$\chi_0(Q) = 2S/[1 - \beta(1 + 2\cos^2 Q)] \tag{4.9}$$

which generates a stable structure for $0 < \beta < 1/3$.

The next stage is essentially a straightforward application of the procedure in § 2. However, there is no frequency dependence in the coefficients in the continued fraction, and we have the recursion relation

$$R_n = \omega R_{n-1} - W_n W_{n-1} R_{n-2} \tag{4.10}$$

generating our generically identical polynomials.

A quantity of interest to any experimental investigation of crystals described by such a Hamiltonian (for example, certain phases in some rare-earth metals) is the dynamic susceptibility, describing the behaviour of fluctuations in the transverse spin components

$$\left|\frac{\mathrm{Im}[G(0,0)]}{\omega}\right| = \begin{cases} -(\chi_0/2)|B_{N-1}|/\sqrt{(L_N)} & L_N \geqslant 0 \\ 0 & L_N < 0 \end{cases} \tag{4.11}$$

$$L_N = 4(W_0 W_1 \ldots W_{N-1})^2 - (A_{N-1} + B_N)^2.$$

This is exactly similar, as one might expect, to the electron density of states (2.3).

5. Results for the spin model

The form of the equations we are dealing with for $\mathrm{Im}\, G_0/\omega$ differ only slightly from those used earlier for the electronic model. Our main numerical problem occurs for zero frequency where, according to whether N is odd or even (Lovesey 1988a), $A_{N-1} + B_N$ may be zero, hence giving a singularity. For ease of computation we remove this feature, which is essentially pathological in nature anyway, whereas the band-edge singularities are formed by the exacting structure of the polynomials.

An additional feature is the dependence on a second parameter k, the external wavevector. We can see intuitively that varying k has a comparatively small effect on the band edges due to the scale imposed on the modulation by β. However, k-dependence can alter the shape of band, particularly at the edge, as the simple $N = 4$ case shows:

$$|(\mathrm{Im}[G(0,0)]/\omega)| \sim 1/[4(1-\beta^2\cos^2(2k)) - \omega^2]^{1/2}. \tag{5.1}$$

Another element to be looked at is the Q numerator, M. We show the spectrum for a series of M/N, with N manageably low (7) to avoid resolution problems (figure 8). Its effect is similar to that of β: to change the band shape and also to introduce possible degeneracy at the band edges.

We also predict a response for the corresponding antiferromagnetic structure:

$$Q' = \pi - Q = 2\pi(N - 2M)/2N. \tag{5.2}$$

For even N this reduces to M'/N, a similar type of spectrum. For odd N, however, our function is controlled by the polynomial L_{2N}, quite different from the ferromagnetic case. In our example, 1/7 gives $Q' = 2\pi(7-2)/14 = 2\pi.5/14$; our corresponding antiferromagnetic state is governed by L_{14}.

The numerical work of Ziman and Lindgard (1986) on this model is based on $Q \sim 2\pi\ 0.12987\ldots$. We present two approximations to this Q, $M/N = 1/8$ (0.125) and 7/54 (~0.12963) (figures 9 and 10). Considering the extremely complicated behaviour of high-order polynomials, we have a great deal of similarity between the three cases (as our Q vectors are all about equal this should be expected!). The fine

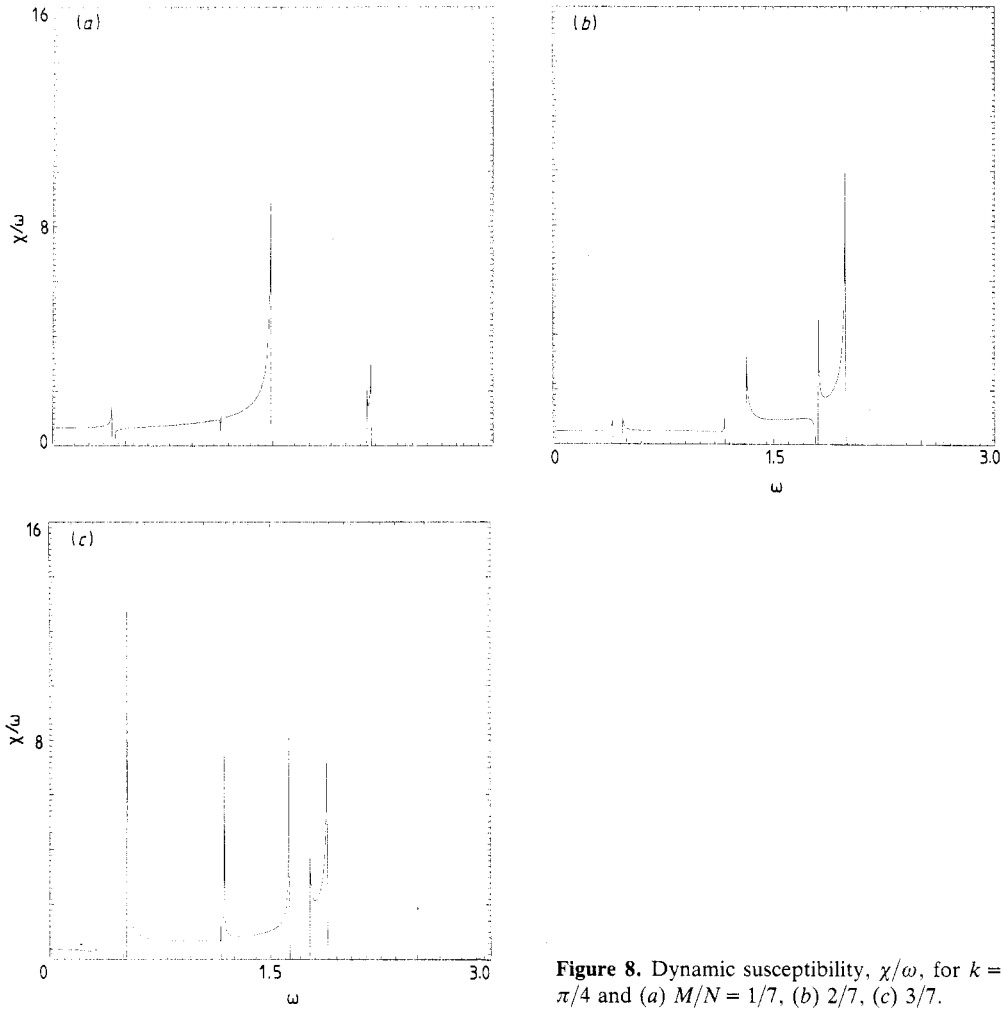

Figure 8. Dynamic susceptibility, χ/ω, for $k = \pi/4$ and (*a*) $M/N = 1/7$, (*b*) 2/7, (*c*) 3/7.

structure that appears with increasing N will not be resolved experimentally. However, the spectrum of spin fluctuations for an incommensurately modulated system is radically different from a commensurate ferromagnetic or antiferromagnetic system in which the response is isolated in the spin dispersion.

6. Discussion

We have implemented the analysis proposed in previous papers to provide detailed pictures of the dynamics of electrons in a rational magnetic field, and spin fluctuations in modulated magnets. A similar discussion of related problems, such as lattice vibrations in a modulated crystal, is a relatively straightforward exercise.

Thus far we have not exploited the formalism to analyse the precise structure of the energy spectrum. Questions of interest in this regard are addressed below.

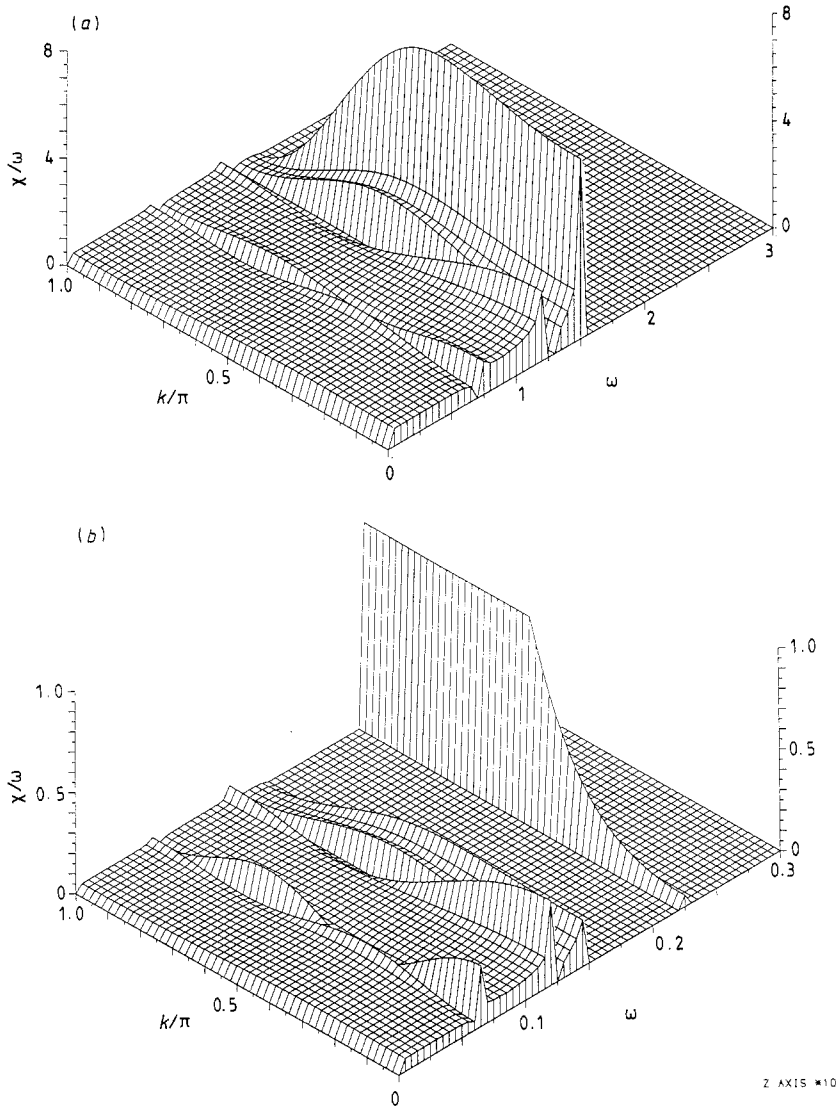

Figure 9. Isometric plots for χ/ω: (*a*) $M/N = 1/8$, (*b*) 7/54; and high-resolution graphs for (*c*) $M/N = 1/8$, $k = 0$, (*d*) 7/54, $k = 0$.

(i) The period-energy butterflies are formed by a Cantor process for a rational fraction Q. But what is the exact relationship between the spectrum of M/N and M'/N'? Can we predict the bands of one knowing the bands of another? There are two consequences of changing the denominator in our formalism. First, the coefficients in θ_N change. As the roots of a polynomial change continuously with a continuous change in its coefficients we might be able to answer this point, but we are also changing the order of our polynomial, which is a discrete change, hence adding greatly to the complexity of the problem.

We know our continued fraction representation is equivalent to that of periodic

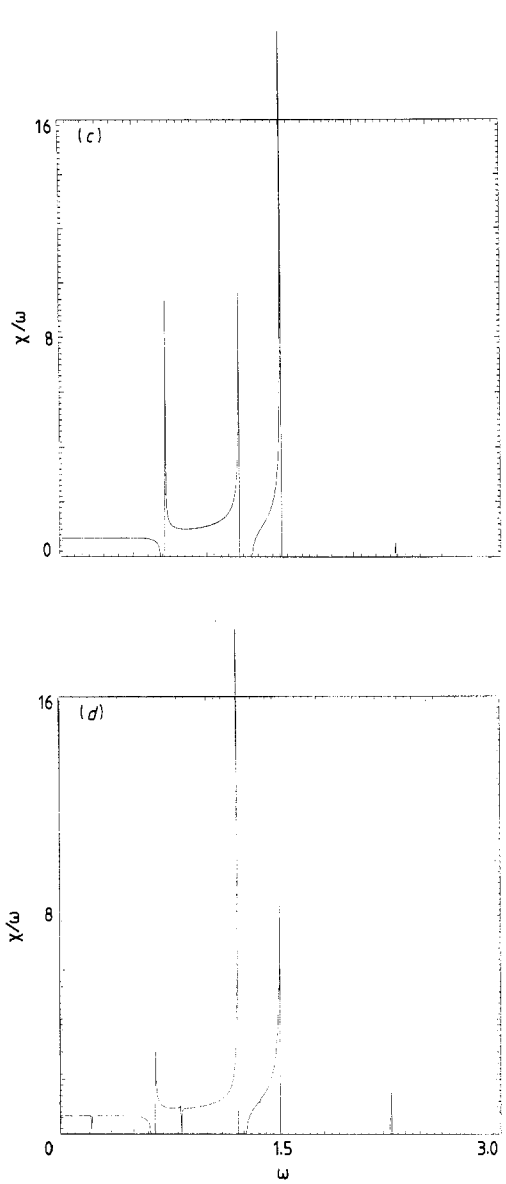

Figure 9. *continued.*

Jacobi matrices, the properties of which have been subject to rigorous investigation in recent years (see, e.g., Kato 1983), and it is in this field that an exacting analysis may yield the hoped-for Cantor form.

(ii) Do our spectra have vanishing measure (do some of the bandwidths vanish) in the incommensurate limit? Investigations by, for example, Janssen and Kohmoto (1988) yield scaling indices for such systems. In a later paper we hope to corroborate their findings.

An example of the spectrum obtained for improved approximations to an irrational modulation wavevector is provided in § 5. For this simple case the structure of the

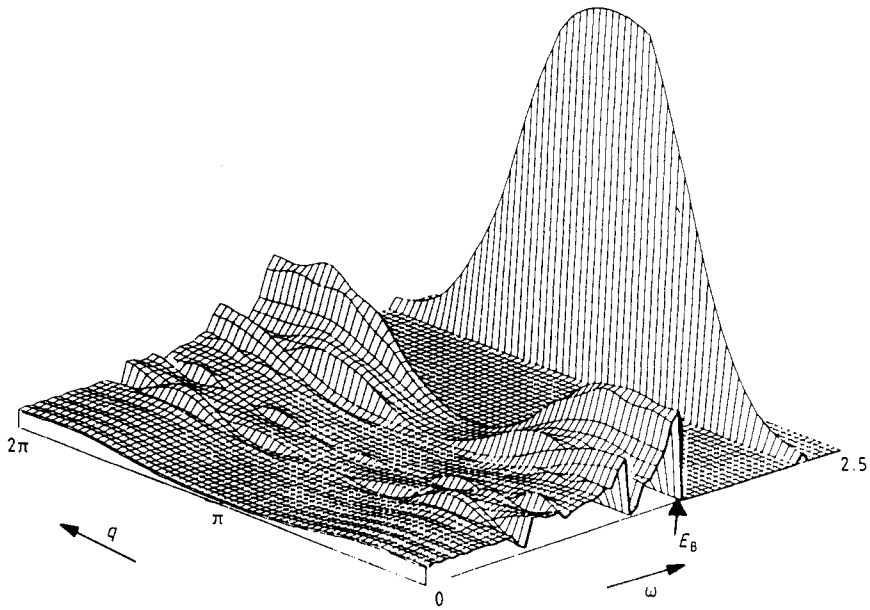

Figure 10. Ziman Lindgard's results for $M/N \sim 0.12987$ ($\mathrm{Im}\,\chi(q, \omega)/\omega$).

response does not change appreciably. We thus are led to expect that after the response function is convoluted with instrumental resolution, it will be difficult to distinguish experimentally between successive approximations for Q.

Acknowledgments

We are grateful to Dr John Chalker for providing useful comments, to Ziman and Lindgard for the use of figure 10, and to Kevin Knowles (RAL) for the help he and his colleagues gave us in presenting the butterflies. MAB also wishes to thank the SERC for a studentship under which this work was carried out.

References

Akhiezer N I 1965 *The Classical Moment Problem* (Edinburgh: Oliver & Boyd)
Currat R and Janssen T 1988 *Solid State Phys.* **41** 201
Elliott R J 1961 *Phys. Rev.* **124** 346
Harper P G 1955 *Phys. Rev.* **124** 346
Harper P G 1955 *Proc. Phys. Soc. London* A **68** 874
Hofstadter D R 1976 *Phys. Rev.* B **14** 2239
Janssen T and Kohmoto M 1988 *Phys. Rev.* B **38** 5811
Kato Y 1983 *Non Linear Integrable Sysatems: Classical Theory of Quantum Theory* ed. M Jimbo and T Niwa (Singapore: World Scientific)
Lovesey S W 1988 *J. Phys. C: Solid State Phys.* **21** 2805
—— 1988 *J. Phys. C: Solid State Phys.* **21** 4967
Simon B 1982 *Adv. Appl. Math,* **3** 463
Sokoloff J B 1985 *Phys. Rep.* **126** 189
Turchi P, Ducastelle F and Treglia G 1982 *J. Phys. C: Solid State Phys.* **15** 2891
Ziman T and Lindgard P A 1986 *Phys. Rev.* B **33** 1976